Applicability of Cytocompatible ALD Barrier Films as Protective Barriers for Biological Implants

A Thesis
Presented to
The Academic Faculty

by

Katarina Adstedt

In Partial Fulfillment
Of the Requirements for the Degree
Materials Science and Engineering, Research Option in the
School of Materials Science and Engineering

Georgia Institute of Technology
Spring 2018

Applicability of Cytocompatible ALD Barrier Films as Protective Barriers for Biological Implants

Approved by:

Dr. Samuel Graham, Advisor
Woodruff School of Mechanical Engineering
Georgia Institute of Technology

Dr. Mark Losego
School of Materials Science & Engineering
Georgia Institute of Technology

Dr. Mary Lynn Realff, Undergraduate Coordinator
School of Materials Science & Engineering
Georgia Institute of Technology

Date Approved: May 4th, 2018

ABSTRACT

The ability of atomic layer deposited (ALD) metal oxide films to serve as protective, encapsulating barriers for biological implants is determined through testing the corrosion resistance and degradation behavior of the films. Using plasma enhanced ALD (PE-ALD), metal-oxides are deposited at 100 ^{o}C onto gold electrodes. Through MTT cell proliferation assay, the films are determined to be cytologically compatible and will not cause harm to the implant host. Using electrochemical impedance spectroscopy (EIS), the films establish their relative chemical stabilities within three different biological environments, phosphate buffer solution (PBS), simulated sweat and simulated saliva. The resulting data from the EIS measurements demonstrates the rate of degradation for the four respective films and exhibits which films are best suited as protective barriers for biological implants. ALD Al_2O_3 is not suitable as an encapsulating layer as it demonstrates no corrosion resistance. Within PBS, ALD TiO_2 establishes itself as the most stable film barrier while within simulated sweat and saliva ALD ZrO_2 is the most chemically stable. The viability of ALD films in biological solutions and their enhanced corrosion resistances opens up the possibility for a new class of materials that can be used for the protection of bioimplants and wearable devices.

Table of Contents

List of Figures

INTRODUCTION

Through the development of flexible, slimmer biological sensors, researchers aim to create wearable and implantable devices with the capability of diagnosing diseases or health issues in a more efficient, timely manner [1]. The improved monitoring capabilities and ease of use of the improved medical devices have resulted in thinner sensors becoming commonplace in the medical market. These devices can range from neural implants to cochlear implants, drug-eluting stents, pacemakers, heart valves and other physiological monitors [2-6]. The biological environments these devices are subjected to can cause degradation or corrosion of the device, prompting the need for a protective barrier.

In order to enable small form factor implantable sensors for biomarker detection, human performance monitoring, and treating diseases, the devices must be either inherently biocompatible or have coatings that prevent the electronics from degrading without negatively affecting the host. Currently, the most common method used for electronic protection is a hermetically packaged, laser-welded enclosure. The limited range of motion from the hermetic packaging inhibits the flexibility of newer medical devices as they conform to the human body [7], prompting the need for newer methods of device protection. The barrier films for biological implants must allow for nominal device operation while providing protection from corrosion without adversely affecting the surrounding cells. It is important for the films to be biocompatible or cytocompatible as they cannot negatively affect their surrounding environments and must ensure safe, long-term operation within the human body [8].

If a medical implant is to be protected from degradation and electrical failure, the barrier coatings must be able to withstand harsh biological environments. Effective barrier coatings are chemically and mechanically stable, biologically compatibly (also known as cytocompatibility), and exhibit low permeability to environmental stressors that could lead to the corrosion or degradation of the devices [9].

High density inorganic barrier coatings, such as metal oxides, prove to be a viable choice as they exhibit excellent gas diffusion barrier properties and ultralow water vapor transmission rates when deposited using atomic layer deposition (ALD) [10]. Other materials (e.g. Teflon, parylenes, diamond-like carbon (DLC) and silicones) have been explored as potential barrier coatings [11-13]. Polymers, although known to be USP Class VI biocompatibility materials with low dielectric constants and high electrical resistance, exhibit high diffusion coefficients, thus rendering them ineffective in biological solutions when compared to inorganics [14]. Of the multiple materials used to establish a biocompatible protective barrier for medical devices, metal oxides, if cytocompatible, will allow for higher corrosion resistances within the films due to their low water vapor transmission rates.

The research gathered by Helmus *et. al*. suggests that biocompatibility can be forced on devices through synthetics, passive and bioactive coatings, and nanomaterials [15]. Many materials have already proven biocompatible behavior, such as Zr and Ti, as shown in research conducted by Izquierdo *et al.* [16]. Beyond coating the device, researchers have developed

biocompatibility through surface modification. In Micksch *et al.*'s study regarding the surface modification of implants, he utilizes specific surface binding peptides in order to determine an adsorption level that proved stable in a biological environment [17]. The peptide sequences adsorbed on ZrO_2, TiZr, and TiO_2 coated sensor chips demonstrated that under stress, the sensors could still function while maintaining biocompatibility, the effects seen through the adhesion and propagation of human mesenchymal stem cells. Not every peptide proved to have a high, stable adsorption level, but those that maintained a high adsorption level demonstrated surface modification as an adequate method to ensure biocompatibility is an intrinsic property of the medical device.

Although surface layer and surface modification prove to be sufficient methods to establish biocompatibility, neither can account for a thin flexible piece of technology that would require biocompatibility to be established on the nanoscale level. As Xie *et al.* [7] discovered in his experiment to determine an encapsulation method that refrained from interfering with the functionality of a device's electrical components, plasma atomic layer deposition (PE-ALD) serves as a new, yet high performing method to establish biocompatibility. PE-ALD is a well-established method of layer-by-layer deposition for protective barriers on polymers, ceramics and other materials. Within Xie *et al.*'s experiment, the encapsulation underwent electrochemical impedance spectroscopy to determine the corrosion resistance, electrical impedance, current leakage, and barrier properties of the film. These variables proved Al_2O_3 and Parylene C layers' effectiveness as encapsulation materials. Xie et al.'s study was conducted over a 24-hour time period. As the films' purpose is to allow long term use of medical devices additional studies to measure corrosion rates must be done over a longer duration.

Within this study, each metal-oxide coating's respective cytocompatibility and degradation behavior is established. Using MTT cell proliferation assay, the viability of the coatings within the human body is established. In order for the films to be considered as potential corrosion barriers, they must not adversely affect the surrounding cells while implanted. All four metal oxides proved to be non-toxic and did not interfere with their surrounding biological environments. Beyond cell compatibility, the corrosion resistance of each film is necessary to understand which films will be more successful than others at protecting the electronic. Using electrochemical impedance spectroscopy (EIS), the chemical stability of Al_2O_3, ZrO_2, HfO_2, and TiO_2 were tested in three different simulated biological environments: phosphate buffer solution (PBS), simulated sweat, and simulated saliva. PBS is a simplified biological environment, mimicking physiological buffers naturally found in the human body. Simulated sweat (artificial perspiration) most closely resembles human eccrine perspiration. Simulated saliva (Fusayama/ Meyer artificial saliva) was chosen based on its primary use for testing biodegradability of dental metal alloys. With the results of this study determined over a 500-hour period, new methods of protecting flexible, biological implants will be established.

METHODS and MATERIALS

Sample Preparation

ALD films were deposited onto gold coated electrodes using plasma enhanced atomic layer deposition (PEALD) system (Cambridge Nanotech, Fiji) at 100°C. For PEALD deposition, trimethyl aluminum (TMA), tetrakis(dimethylamido) hafnium (TDMAH), tetrakis(dimethylamido) titanium (TDMAT), and tetrakis(dimethylamido) zirconium (TDMAZ) were the precursors for the deposition of Al_2O_3, HfO_2, TiO_2 and ZrO_2, respectively. Oxygen plasma was used for 20 seconds as an oxidizer with plasma power of 300 W. The thicknesses of ALD films were measured using Woollam M2000 ellipsometer by depositing them on silicon substrate.

The solutions utilized in this experiment were PBS, simulated saliva, and sweat. PBS was obtained in powder form from Amresco and the PBS solution with strength of 1x was prepared by dissolving 9.88g of powder in 1L deionized water. Both the simulated sweat and simulated saliva solutions were provided by Pickering Laboratories, Inc. Simulated saliva (Fusayama/ Meyer Artificial Saliva) consisted of 97-100% deionized water, ≤ 1.0% KCl, ≤ 0.5% urea, ≤ 0.1% NaCl, ≤ 0.1% sodium phosphate monobasic dehydrate, ≤ 0.1% calcium chloride dehydrate, and ≤ 0.0005% sodium sulfide nonahydrate. Simulated sweat (Artificial Perspiration, DIN 53160-2:2010/BS EN 1811:2011) consisted of 98-99% deionized water, ≤ 1.0% NaCl, ≤ 0.5% urea, and ≤ 0.5% lactic acid.

Cytocompatibility

MTT crystal was purchased from biotium (Cat:30006). DMEM and calf serum were purchased from ATCC. The cytotoxicity evaluation of ALD materials was performed with (3-(4,5-Dimethylthiazol-2-yl)-2,5-Diphenyltetrazolium Bromide) (MTT) assay. Coverslips coated with HfO_2, Al_2O_3, ZrO_2 and TiO_2 were sterilized under UV for 30min and then carefully moved to 24 well plates. NIH-3T3 (passage 100) were seeded on top of the coated coverslips at density of 50,000/well in complete medium (DMEM with 10% calf serum). MTT assay were performed according to manufacturer's protocol.

Cell mediums were removed after culturing for 18h at 37˚C (5% CO_2). MTT reagent was added to each well within the well plate according to manufacturer's protocol. After 2h incubation, double volume of DMSO was added to each well and pipette up and down several times to dissolve the formazan salt. Upon mixture, the absorbance signal was measured on a plate reader (BioTek Synergy H4) at 570nm (signal) and 630nm (background). Normalized absorbance values were obtained by subtraction background absorbance (630nm) from signal absorbance (570nm).

Corrosion Resistance

Electrochemical impedance spectroscopy (EIS) measurements were performed using a Reference 600™ potentiostat from Gamry Instruments. Custom built electrochemical cells were

used for taking electrochemical impedance measurements. The schematic of the cell is shown in Figure 1. The electrical contacts were made from top of the electrode while solution the bottom half of the electrode. The area of the electrode submerged into the solution is 4.17 cm^2. EIS measurements were conducted in phosphate buffer saline (PBS) solution, simulated saliva and sweat solutions by applying a frequency range from 10^{-1} to 10^5 Hz and an amplitude of 10 mV. The measurements were taken at regular intervals over a period of 500-hours.

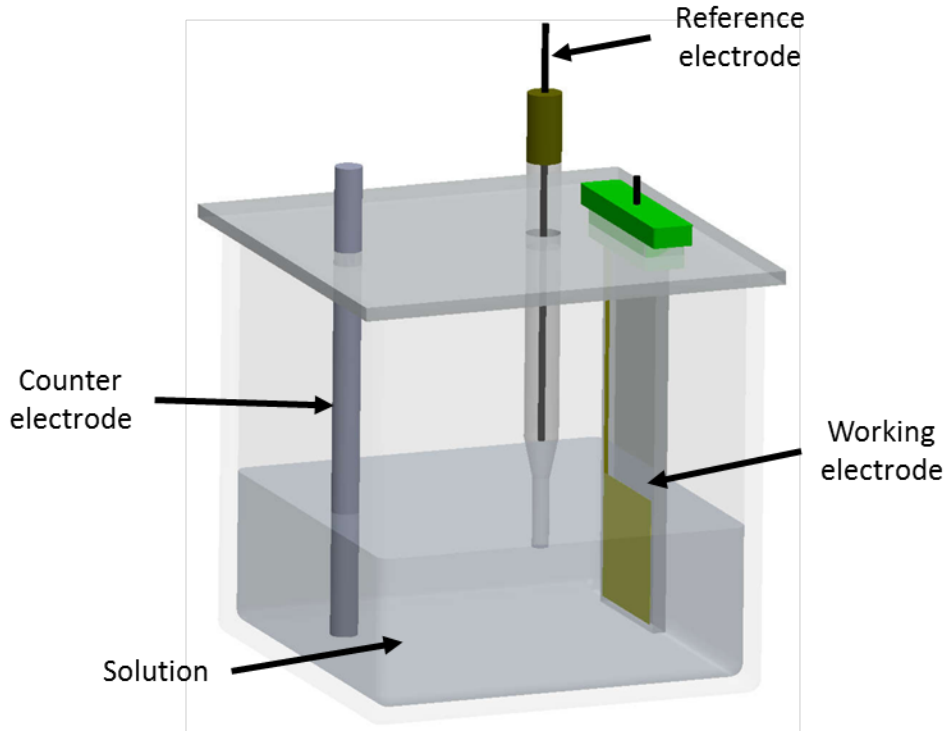

Figure 1. EIS Setup

Surface Characterization

Chemical characterization of the ALD films were conducted with X-ray photoelectron spectroscopy (XPS) on a Thermo Scientific K-Alpha X-ray photoelectron spectrometer system with a monochromatic Al K_α X-ray source (hν = 1486.6 eV). The chemical state of the ALD materials was determined before and after exposure to the solutions for 500 hours. To compensate for charging effect, all the XPS spectra were shifted with respect to adventitious carbon (C1s) peak at 284.8 eV.

RESULTS

Cytocompatibility

To test the cytocompatibility of ALD materials, a MTT based in vitro cytotoxicity study was performed with NIH-3T3 cells culturing on ALD coated slides for 18 hours. To compare each of the experimental groups (cells culturing on ALD coated slides) with control group (cells

culturing on plain tissue culture plates), Dunnett's statistics test was performed with one-way ANOVA multiple comparison. No significant difference in cell viability was observed, as shown in Figure 2.

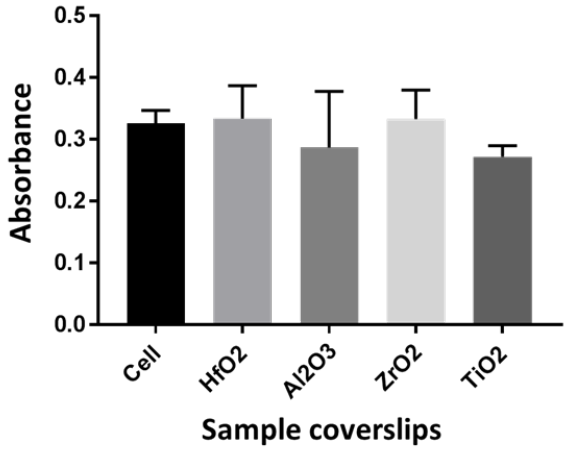

Figure 2. Normalized absorbance intensity of 570 nm wavelength through the control and ALD coated coverslips

EIS Measurements

1. *ALD Films in PBS*

The bode plots of ALD films in PBS solution are shown in Figure 3. The inset in the figures represent phase change plots of first and last measurement for the respective materials. For ALD Al_2O_3, there is high impedance in low frequency regions as seen in the inset of Figure 3(a). Figure 3(b) shows the bode plots for ALD HfO_2 in PBS solution. There is not significant difference in the initial and final impedance plots of the ALD HfO_2 layer.

Figure 3(c) shows the bode plots for ALD TiO_2 in PBS solution. The plots demonstrate no significant change in impedance response of the sample with time. All the impedance plots appear to overlap indicating that there is no significant change in the material with time. Figure 3(d) shows the bode plots for ALD ZrO_2 in PBS solution. The impedance response from the ALD ZrO_2 material has changed with time, there is more widening between the impedance plots in the low frequency region.

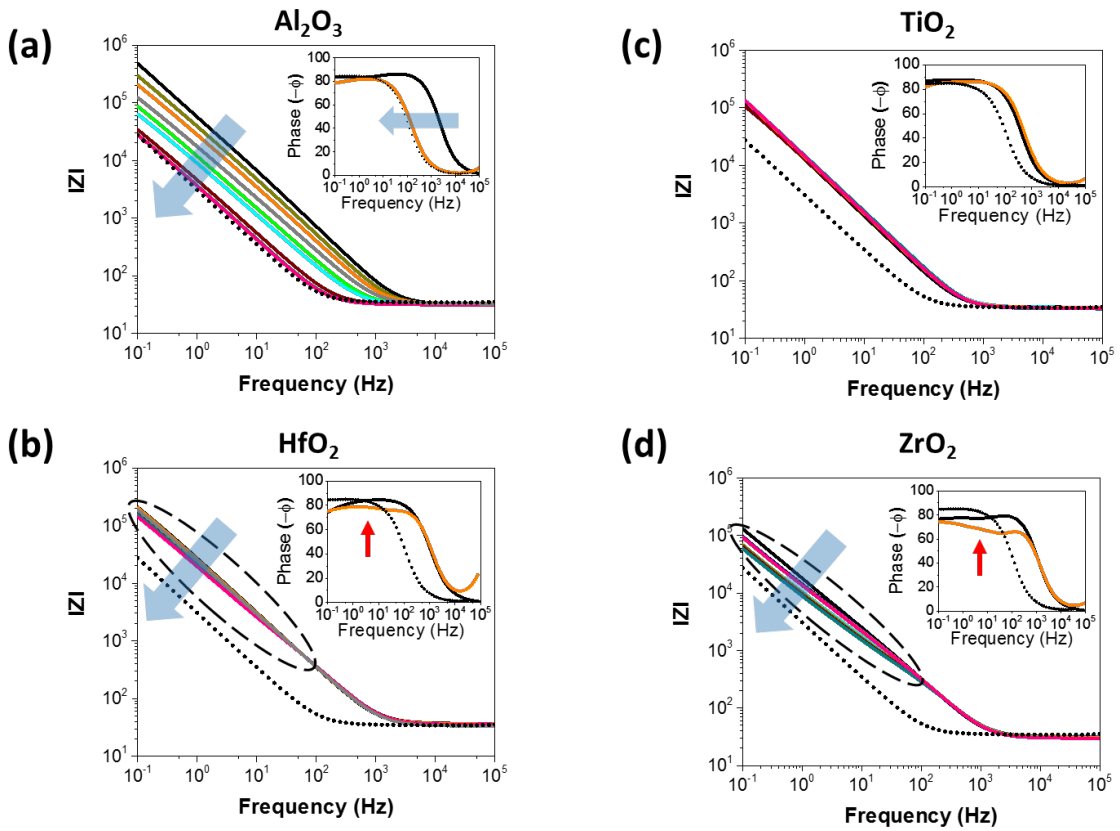

Figure 3. EIS response in PBS solution for (a) Al_2O_3, (b) HfO_2, (c) TiO_2, and (d) ZrO_2 over a time period of 500-hours. Dotted line represents impedance response from bare electrode. Blue arrows point towards the direction of measured data. Insets in the figure represent phase response for first and last measurement. Red arrow point towards the appearance of second time constant in the phase plots.

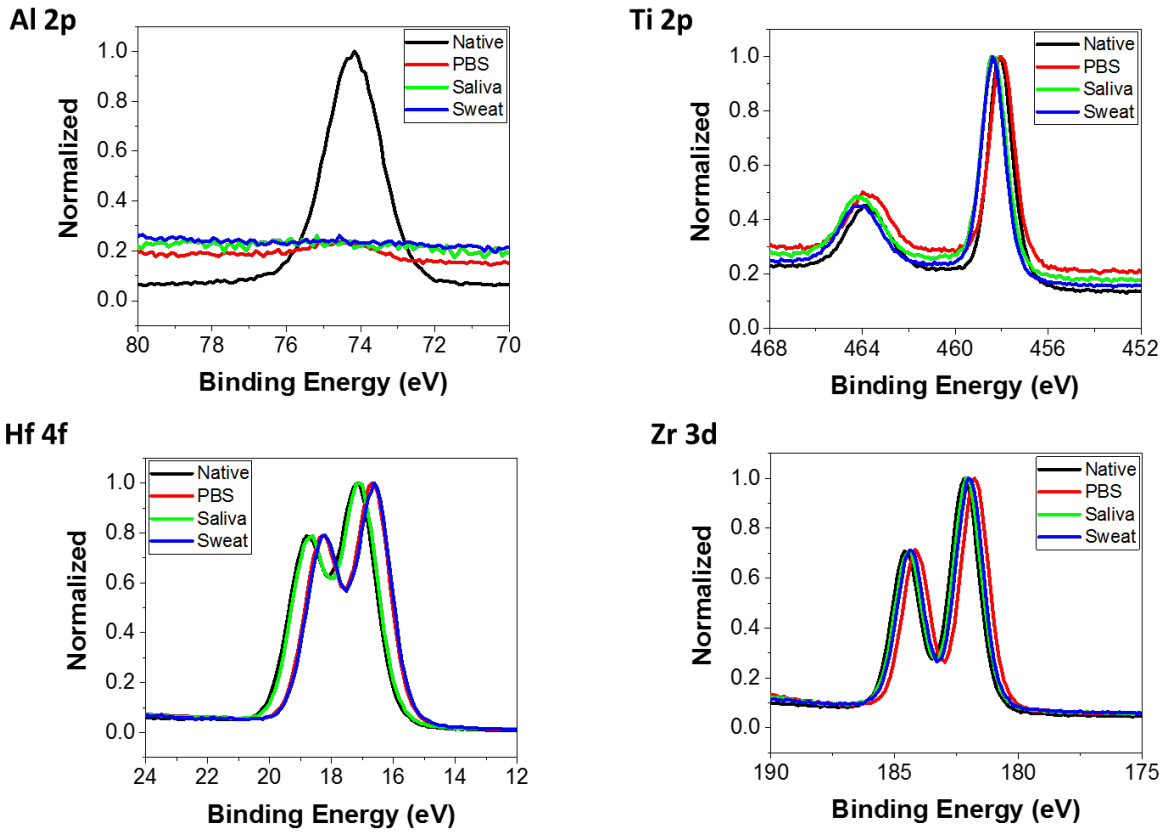

Figure 4. XPS spectra of metallic elements. Color code: Black represents binding energy for native samples (before exposure) to biological solutions. Red, green and blue represent binding energy for samples in PBS, saliva and sweat after exposure for 500-hours, respectively.

2. *ALD Films in Saliva*

The bode plots for the ALD films in saliva solution are shown in Figure 5. The inset in the figures represent phase change plots of initial and last measurement for respective materials. For ALD Al_2O_3, there is high impedance in the low frequency region as seen in the Figure 5(a). After day 1, there is sudden change in the impedance response of the ALD Al_2O_3 material. Figure 5(b) shows the bode plots for ALD HfO_2 in saliva solution. With exposure of the film to saliva solution, there is a change in impedance response.

Figure 5(c) shows the bode plots for ALD TiO_2 in saliva solution. The plots demonstrate a slight change in impedance response of the sample with time. When comparing the impedance response of the material over 500 hours, it is evident from the inset of Figure 5(c) that there is widening in impedance response on either side of ~5 Hz frequency.

Figure 5(d) shows the bode plots for ALD ZrO_2 in saliva solution. The impedance response from the ALD ZrO_2 material has no noticeable change with time. From inset in

the Figure 5(d), it is evident that there is no significant change in the time constant for last measurement as compared to the initial measurement.

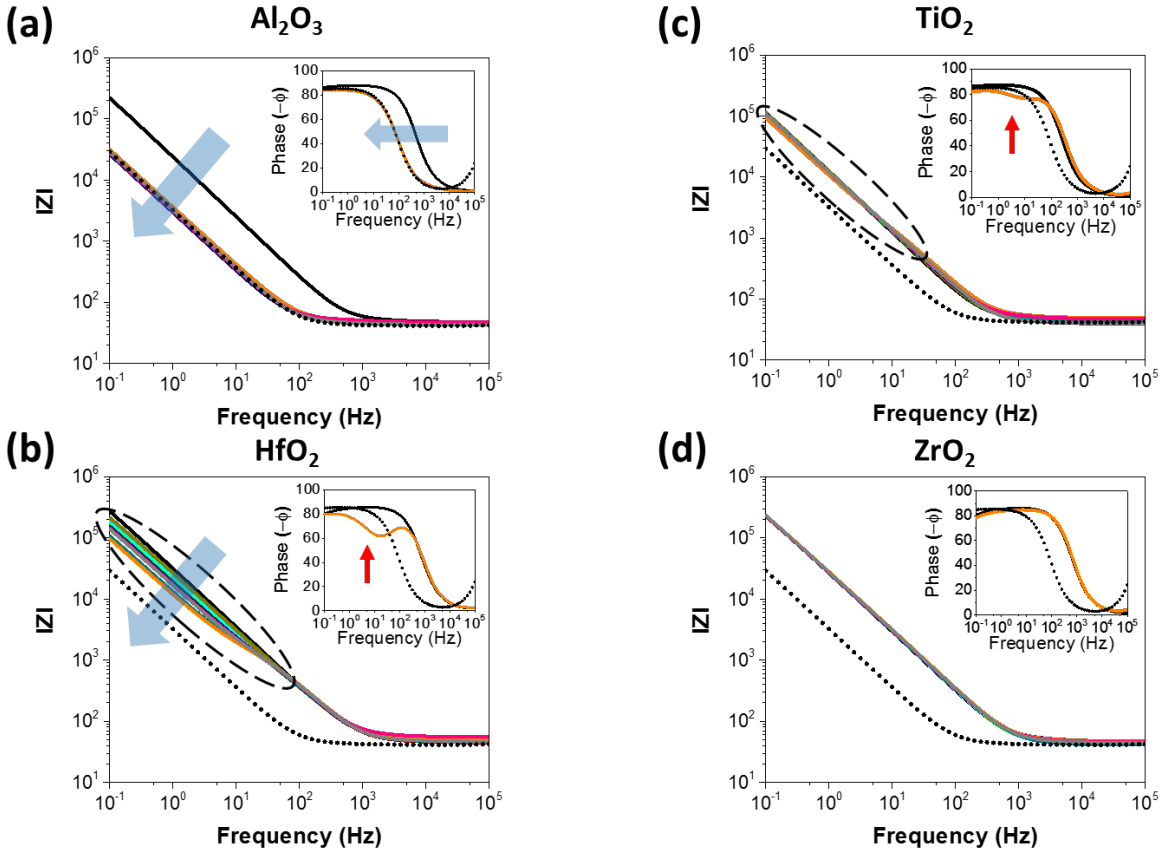

Figure 5: EIS response in saliva solution for (a) Al_2O_3, (b) HfO_2, (c) TiO_2, and (d) ZrO_2 over a time period of 500 hours. Dotted line represents impedance response from bare electrode. Blue arrows point towards the direction of measured data. Insets in the figure represent phase response for first and last measurement. Red arrow point towards the appearance of second time constant in the phase plots.

3. *ALD Films in Sweat*

The bode plots of the ALD films in sweat solution are shown in Figure 6. For ALD Al_2O_3, similar to that of other two solutions, there is high impedance in low frequency region as shown in the Figure 6(a). Figure 6(b) shows the bode plots for ALD HfO_2 in sweat solution.

Figure 6(c) shows the bode plots for ALD TiO_2 in sweat solution. With exposure of the material to sweat solution, the impedance response from the ALD material changes in the lower frequency region. Figure 6(d) shows the bode plots for ALD ZrO_2 in sweat solution. With exposure of the ALD film to sweat solution, a continuous change in the impedance spectra was observed with time.

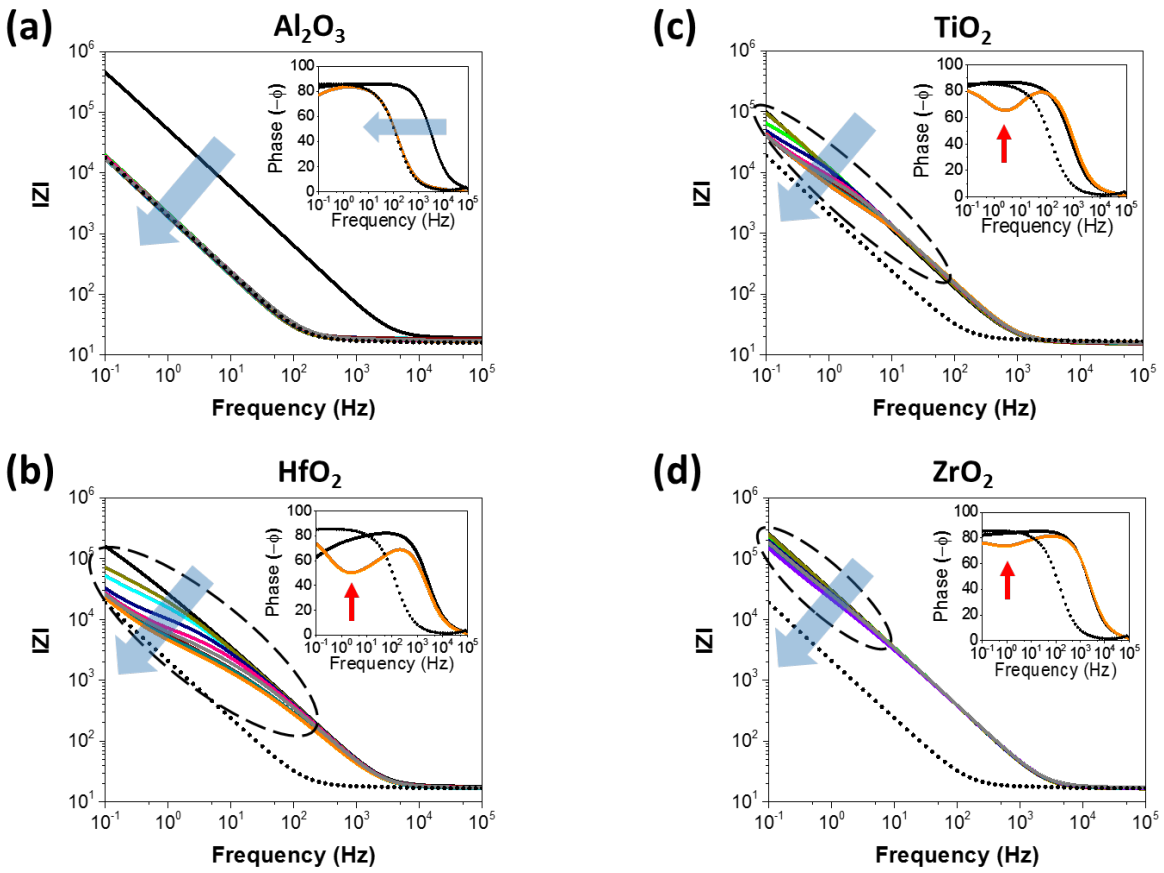

Figure 6: EIS response in sweat solution for (a) Al_2O_3, (b) HfO_2, (c) TiO_2, and (d) ZrO_2 over a time period of 500 hours. Dotted line represents impedance response from bare electrode. Blue arrows point towards the direction of measured data. Insets in the figure represent phase response for first and last measurement. Red arrow point towards the appearance of second time constant in the phase plots.

DISCUSSION

Cytocompatibility

Due to the negligible difference in the cell viability observed for the 4 ALD materials, the metal-oxide coatings have no cytotoxicity effect. Therefore, all of the ALD coatings chosen for this study demonstrate cytocompatibility for use in devices exposed to biological environments.

EIS

1. *ALD in PBS*

With prolonged exposure of ALD Al_2O_3 to the PBS solution, there is a continuous decrease in the impedance of the film in the lower frequency regime, approaching the impedance of the bare electrode, as shown in Figure 3(a). The minimum value was obtained on the 22nd measurement at 500 hours. Similar tendency was observed for phase shift as well. The phase response of the ALD Al_2O_3 shifted towards that of the bare

electrode on last day of measurement. This indicates that there is a continuous thinning of the ALD Al_2O_3 layer due to dissolution of the material into the PBS solution. The XPS data for ALD Al_2O_3 in PBS solution is shown in Figure 4(a). It is clear from the XPS data that the intensity of Al2p peak has reduced significantly and only traces of Al_2O_3 remain on the electrode surface. The peaks from the electrode material, i.e. Ti and Au (not shown), were clearly visible, conforming the removal of ALD Al_2O_3 from the electrode surface.

With exposure of the ALD HfO_2 film to saliva solution, there is a change in impedance response indicating degradation of the material as shown in the encircled region of Figure 3(b) with the widening in the gap between impedance plots in the low frequency region (below ~50 Hz). The widening in the impedance response at lower frequencies and appearance of an additional time constant indicates the formation of a new capacitive area in the sample, diverging from the initial, uniform film. However, after exposure to the PBS solution, degradation started in the material. The XPS data revealed that there is a peak shift in the binding energy of Hf4f indicating a chemical change in the ALD material, as shown in Figure 4. This is consistent with the results from EIS where there some change in the material was observed. While broadening in the low frequency region, the impedance data shift towards that of the bare electrode indicating that the newly formed region is thinner than other regions of ALD HfO_2. This means that the degradation of the ALD HfO_2 is not uniform as that of ALD Al_2O_3. Instead, localized degradation or thinning occurred in the HfO_2 layer which could be the result of selective etching of the material near the defect sites.

The phase plot of ALD TiO_2 taken after 500 hours of exposure to PBS overlaps with the first measurement plot indicating that ALD TiO_2 is stable in PBS solution. This is also supported by overlap in binding energy peaks for Ti2p before and after exposure to PBS for 500 hours, as shown in Figure 7.

The formation of second region of thickness different from rest of the material in ALD ALD ZrO_2 is supported by the appearance of second time constant in the phase response of ALD ZrO_2 as shown in the Figure 3(d). This means that there is localized degradation of the material. XPS data revealed that there is a shift in binding energy for Zr3d peaks, as shown in Figure 3(d), resulting from change in chemical state of Zr in ALD ZrO_2.

2. *ALD in Saliva*

The impedance from the sample matches to that of the bare electrode indicating that ALD Al_2O_3 was completely removed from the substrate surface. As shown in the inset of Figure 5(a), the phase change plot for ALD Al_2O_3 after 500 hours overlaps to that of the electrode. The XPS spectra taken for this sample after 500 hours show that there is no trace of Al on substrate surface as shown in Figure 7(a). Only the peaks for Ti and Au from the electrode were obtained which is consistent with the observation from EIS data.

Thus, ALD Al_2O_3 got completely dissolved into the saliva solution within a day, such that no intermediate step could be detected. This means that ALD Al_2O_3 is highly unstable in saliva solution.

When comparing the data taken over a period of 500 hours, it is evident that in the middle region of frequency (~100 Hz), the impedance plots overlap throughout the measurement period as shown in the Figure 5(b). However, there is a continuous widening in the gap between the impedance plots at lower frequency region. From the inset in the Figure 5(b), it is seen that there are two time constants as opposed to only one in case of first measurement. The XPS spectra taken for ALD HfO_2 after 500 hours of exposure to saliva solution shows that there is a shift in peak of Hf4f towards lower binding energy. The shift towards a lower binding energy of the ALD HfO_2 material means that HfO_2 is not entirely stable, chemically, in the saliva solution. However, the rate of chemical degradation of the material is not as fast as that of ALD Al_2O_3. As indicated by the EIS and XPS data, ALD HfO_2 gets dissolved into the solution resulting into the thinning of the ALD layer. However, non-uniform decrease in thickness of the material means that there is selective etching or removal of ALD HfO_2. This could be the result of presence of highly vulnerable sites near the proximity of pinholes and other defects.

The widening of the impedance response indicates the formation of two different regions in the sample which should have two different time constants. This is confirmed by the phase change plot in the inset of Figure 5(c) where there is appearance of two time constants. This could be the result of slow degradation of ALD TiO_2 at some selective regions in saliva solution. XPS data reveals that there is an increase in binding energy of Ti on exposure to saliva indicating towards the chemical interaction between the ALD TiO_2 and components of saliva solution. Thus, XPS data supports the conclusion from EIS data of having change in the state of TiO_2 material. Since there is formation of two regions with different thicknesses, the decrease in thickness of the sample in certain regions could be due to the rapid degradation at highly vulnerable sites near the defects in the layer.

The negligible change in impedance response for ALD ZrO_2 in simulated saliva indicates that there is no apparent dissolution of ALD ZrO_2 into the surrounding media. However, as per XPS data, there is a change in peak position for binding energy of Zr3d towards lower value indicating a change in chemical state of ZrO_2 at the surface. But, consistent impedance response from the material throughout the experiment duration indicates that the newly formed material does not get dissolved into the saliva solution and thus get removed from the substrate surface. Thus, ALD ZrO_2 can be considered to be a highly stable material in saliva solution.

3. *ALD in Sweat*

With exposure of ALD Al_2O_3 to the sweat solution, a sudden change in impedance behavior of the film, similar to that in the saliva solution, was observed. The second impedance measurement, taken 48 hours after first measurement and exposure to simulated sweat, shifted significantly towards lower frequency overlapping with that of the bare electrode. The significant shift of the impedance plot towards the bare electrode means that there was complete removal of ALD Al_2O_3 within a day. From second measurement onwards, all the impedance data overlapped. XPS data, shown in Figure 7, shows that there is no trace of Al on the substrate which is consistent with the observation from EIS that the complete removal of ALD Al_2O_3 has taken place. Therefore, it can be concluded that ALD Al_2O_3 dissolved completely into the surrounding media within a day. After this, there was no material remaining on electrode surface for further dissolution and hence, no change in the impedance response from the sample was observed after day 1 onwards. Thus, ALD Al_2O_3 is highly unstable in simulated sweat solution.

With exposure of the film to sweat solution, the impedance response changes for ALD HfO_2, as shown in Figure 6(b). When comparing the data taken over the period of 500 hours, it is evident in the middle to low frequency regime (below ~100 Hz) that the impedance plots start to diverge greatly throughout the measurement period. The formation of a region in the ALD HfO_2 sample which has different thickness than rest of the sample is supported by the presence of two time constants for the sample after 500 hours as shown in the inset of the Figure 6(b). The thinning in the HfO_2 layer could be the result of dissolution of material into the solution. XPS analysis of the surface after 500 hours, as shown in Figure 7(b), revealed that there is a shift in binding energy for Hf4f, indicating a change in chemical state of the ALD material. This signifies possible dissolution of HfO_2 into the solution as a result of chemical interaction with the surrounding species. Thus, HfO_2 is not stable in sweat solution.

In Figure 6(c), widening in the gap between impedance plots can be observed with time in the region below the frequency of ~10 Hz, The widening gap between impedance plots for ALD TiO_2 indicates the formation of a region with thickness different than rest of the material, similar to that of ALD HfO_2. This is supported by the presence of second time constant in the inset of the Figure 6(c). As the impedance plot in low frequency region tends to shift towards that of the bare electrode, it can be concluded that there is thinning in the material thickness in some parts of the sample. The decrease in thickness of the sample could be due to the formation of defects and removal of material from the ALD layer. The XPS spectra, as shown in Figure 7, shows that there is a peak shift in the binding energy of Ti2p peaks. This implies that there is chemical interaction between ALD TiO_2 and the surrounding species which could have resulted in dissolution of the material into the solution, leading to thinning of the ALD layer. As per impedance data, the change in thickness of TiO_2 is not uniform throughout the sample. This means that the rate of decrease in thickness of the TiO_2 layer is higher at sites in the proximity of defects. Since the broadening in the impedance peak in case of TiO_2 was smaller than that of HfO_2, it can be concluded that TiO_2 is more stable in sweat.

From Figure 6(d), it is evident that there is widening in the gap between the impedance plots for the frequencies below ~10 Hz. The widening between impedance measurements at low frequencies for ALD ZrO_2 indicates the formation of a region which has thickness different than rest of the sample, similar to that of HfO_2 and TiO_2. The existence of two regions with different thicknesses is supported by the presence of second time constant for impedance data on the 22^{nd} measurement at 500 hours. Since the impedance response of the ALD material in lower frequency regions tends to approach that of the bare electrode, it can be concluded that the new region formed has a thickness smaller than the initial thickness of the sample. The XPS data revealed that there is a change in peak position for the binding energy of the Zr3d on exposure to sweat solution for 500 hours. This means that there is some chemical interaction between ALD ZrO_2 and the surrounding solution leading to dissolution of the material into the solution. This results in thinning of the ALD layer as indicated by the impedance data. As the decrease in thickness is not uniform throughout the ALD layer, localized thinning in selective regions of the sample could be suspected. This localized thinning in the ALD layer can be associated to the defects in the film which make the areas of the film in their proximity to be highly vulnerable to attack from the solution. Although, ZrO_2 might have shown some degradation in sweat solution, it is found to be more stable than the other three ALD materials under consideration for this study.

CONCLUSION

A biocompatible, protective barrier for electronic medical implants may improve the lifetime of the device. Through the experiment, all four metal oxides were proven to be cytocompatible through MTT cell proliferation assay. Of the four metal oxides, ALD Al_2O_3 proved to be an unstable choice in all three solutions for long-term protection of a biological implant. In both simulated sweat and saliva, there was no Al_2O_3 remaining after 24 hours of exposure while in PBS there was a constant degradation of the barrier until no Al_2O_3 is remaining. The other metal oxides, TiO_2, ZrO_2, and HfO_2, demonstrated varying levels of protection while submerged in three different simulations of the human body. ALD TiO_2 demonstrated the highest success at long-term protection in PBS while ALD ZrO_2 was the most stable in simulated sweat and saliva. Using ALD ZrO_2 and TiO_2, the viability of the barrier coatings will be demonstrated on a flexible silver electrode. Through the viability study, the applicability of the ALD metal oxides will establish their ability to sustain the electronics' performance. The ALD metal oxide protective barriers are an opportunity to maintain the functionality of biological implants while protecting them from the harsh environments of the human body.

REFERENCES

[1] Luo, N.Q., et al., *Mobile Health: Design of Flexible and Stretchable Filectrophysiological Sensors for Wearable Healthcare Systems.* 11th International Conference on Wearable and Implantable Body Sensor Networks (Bsn), 2014: p. 87-91.

[2] Greatbatch, W. and C.F. Holmes, *History of implantable devices.* IEEE Engineering in Medicine and Biology Magazine, 1991. **10**(3): p. 38-41.

[3] Hassarati, R.T., et al., *Improving cochlear implant properties through conductive hydrogel coatings.* IEEE Trans Neural Syst Rehabil Eng, 2014. **22**(2): p. 411-8.

[4] Alves, P., et al., *Surface modification of polyurethane films by plasma and ultraviolet light to improve haemocompatibility for artificial heart valves.* Colloids Surf B Biointerfaces, 2014. **113**: p. 25-32.

[5] Ma, X., et al., *Drug-eluting stents.* International Journal of Clinical and Experimental Medicine, 2010. **3**(3): p. 192-201.

[6] Hwang, G.-T., et al., *Self-Powered Cardiac Pacemaker Enabled by Flexible Single Crystalline PMN-PT Piezoelectric Energy Harvester.* Advanced Materials, 2014. **26**(28): p. 4880-4887.

[7] Xie, X., et al., *Long-Term Bilayer Encapsulation Performance of Atomic Layer Deposited Al2O3 and Parylene C for Biomedical Implantable Devices.* IEEE Transactions on Biomedical Engineering, 2013. **60**(10): p. 2943-2951.

[8] Anderson, J.M., *Biological Responses to Materials.* Annual Review of Materials Research, 2001. **31**(1): p. 81-110.

[9] Bazaka, K. and M. Jacob, *Implantable Devices: Issues and Challenges.* Electronics, 2012. **2**(1): p. 1-34.

[10] Carcia, P.F., et al., *Ca test of Al2O3 gas diffusion barriers grown by atomic layer deposition on polymers.* Applied Physics Letters, 2006.

[11] Lago, N., et al., *Long term assessment of axonal regeneration through polyimide regenerative electrodes to interface the peripheral nerve.* Biomaterials, 2005.

[12] Roy, R.K. and K.R. Lee, *Biomedical applications of diamond-like carbon coatings: A review.* Journal of Biomedical Materials Research Part B-Applied Biomaterials, 2007.

[13] Hsu, J.M., et al., *Characterization of a-SiCx : H thin films as an encapsulation material for integrated silicon based neural interface devices.* Thin Solid Films, 2007.

[14] Wasikiewicz, J.M., et al., *Polymeric barrier membranes for device packaging, diffusive control and biocompatibility.* Applied Surface Science, 2008. 255(2): p. 340-343.

[15] Helmus, M.N., D.F. Gibbons, and D. Cebon, *Biocompatibility: Meeting a Key Functional Requirement of Next-Generation Medical Devices.* Toxicologic Pathology, 2008. **36**(1): p. 70-80.

[16] Izquierdo, J., et al., *Electrochemical characterization of pulsed layer deposited hydroxyapatite-zirconia layers on Ti-21Nb-15Ta-6Zr alloy for biomedical application.* Applied Surface Science, 2016. **385**: p. 368-378.

[17] Micksch, T., et al., *Investigation of the Peptide Adsorption on ZrO2, TiZr, and TiO2 Surfaces as a Method for Surface Modification.* Acs Applied Materials & Interfaces, 2014. **6**(10): p. 7408-7416.